Topological Magnetic Insulators with Corundum Structure

Jing Wang, Rundong Li, Shou-Cheng Zhang, and Xiao-Liang Qi

Phys. Rev. Lett. **106**, 126403 — Published 24 March 2011

DOI: 10.1103/PhysRevLett.106.126403

Topological Magnetic Insulators with Corundum Structure

Jing Wang,[1,2] Rundong Li,[2] Shou-Cheng Zhang,[2] and Xiao-Liang Qi[3,2]

[1]*Department of Physics, Tsinghua University, Beijing 100084, China*
[2]*Department of Physics, McCullough Building, Stanford University, Stanford, CA 94305-4045*
[3]*Microsoft Research, Station Q, Elings Hall, University of California, Santa Barbara, CA 93106*

Topological insulators are new states of quantum matter in which surface states residing in the bulk insulating gap are protected by time-reversal symmetry. When a proper kind of antiferromagnetic long range order is established in a topological insulator, the system supports axionic excitations. In this paper, we study theoretically the electronic states in a transition metal oxide of corundum structure, in which both spin-orbit interaction and electron-electron interaction play crucial roles. A tight-binding model analysis predicts that materials with this structure can be strong topological insulator. Because of the electron correlation, an antiferromagnetic order may develop, giving rise to a topological magnetic insulator phase with axionic excitations.

PACS numbers: 71.70.Ej, 75.30.Kz, 75.80.+q, 73.20.-r

The discovery of time reversal invariant topological insulator has attracted great attention in condensed matter physics [1–9]. With time-reversal symmetry broken on the surface, the electromagnetic response of three dimensional (3D) insulators are described by the topological θ term of the form $S_\theta = (\theta/2\pi)(\alpha/2\pi)\int d^3x dt \mathbf{E}\cdot\mathbf{B}$ together with the ordinary Maxwell terms, where $\mathbf{E}$ and $\mathbf{B}$ are the conventional electromagnetic field insides the insulator, $\alpha = e^2/\hbar c$ is the fine structure constant, and θ is the dimensionless pseudoscalar parameter describing the insulator, which refers to "axion" field in axion electrodynamics [10]. For a system without boundary, all the physical quantities are invariant if θ is shifted by integer multiple of 2π. Therefor all time reversal invariant insulator fall into two distinct classes described by either $\theta = 0$ (trivial insulator) or $\theta = \pi$ (topological insulator)[11]. Such a universal value of $\theta = \pi$ in topological insulators leads to magneto-electric effect with an universal coefficient, which has several unique experimental consequences such as a topological contribution to the Faraday rotation or Kerr rotation[11–13], and the image monopole induced by an electron[14]. θ has an explicit microscopic expression of the momentum space Chern-Simons form which depends on the band structure of the insulator [11]

$$\theta = \frac{1}{4\pi}\int d^3k\epsilon^{ijk}\mathrm{Tr}\left[A_i\partial_j A_k + i\frac{2}{3}A_iA_jA_k\right], \quad (1)$$

where $A_i^{\mu\nu}(\mathbf{k}) = -i\langle u_\mu|\partial/\partial k_i|u_\nu\rangle$ is the momentum space non-abelian gauge field, with $|u_\mu\rangle$, $|u_\nu\rangle$ referring to the Bloch wavefunction of occupied bands.

If strong electron correlation exists in a topological insulator, a long-range antiferromagnetic(AFM) order can be established under enough low temperature. Since the AFM order breaks time-reversal symmetry spontaneously, θ can deviate from π, and also becomes a *dynamical* field which has fluctuations associated with some spin collective modes. The spin collective mode inducing fluctuations of θ are thus coupled to the photons by $\theta\mathbf{E}\cdot\mathbf{B}$ term, which means they become "axions" in the term used in high energy physics. Such a nonconventional antiferromagnetic insulator supporting axion excitations is proposed as topological magnetic insulator (TMI) [15]. Due to its coupling to photons, the axion field hybridizes with photons, leading to axion polariton, with a polariton gap tunable by an external magnetic field. Thus such a material can be used as a novel type of optical modulator to control the transmission of light through the material.

To realize the TMI phase, we need both the nontrivial topology of the electron bands and strong electron correlation. The materials with electrons in 3d, 4d or 5d-orbital can have both strong spin-orbit coupling (SOC) and strong interaction, which is ideal for this purpose. Recently, models for topological insulators with strong electron correlation have been proposed[16–19], also topological phases may exist in thallium-based III-V-VI_2 ternary chalcogenides[20] as well as ternary heusler compounds[21, 22]. In this Letter, we study theoretically the transition metal oxide ABO_3 of corundum structure with A and B standing for some transition metals such as Fe, Ru, Rh, Ir, Os, etc [23]. A possible candidate material is α-Fe_2O_3. A tight binding model is obtained by using point group symmetry of this structure, from which we find a TMI phase with certain SOC strength and electron-electron interaction.

The corundum structure is shown in Fig. 1(a). Each transition metal atom is surrounded by oxygen octahedron, and the d orbitals are split by the octahedral crystalline field into doublet $e_g(x^2-y^2, 3z^2-r^2)$ and triplet $t_{2g}(xy, yz, zx)$ orbitals (See Fig. 1(c)). We will neglect small distortion of the oxygen octahedra which may lead to minor corrections to electronic structure [24]. The energy of t_{2g} stays lower with respect to e_g, because the latter point towards the negatively charged oxygens. The SOC is effective in t_{2g} orbitals and negligible in e_g orbitals. Including the SOC, t_{2g} splits into total angular momentum $j_{\text{eff}} = 3/2$ and $j_{\text{eff}} = 1/2$. We focus on those materials where the Fermi level lies completely in the

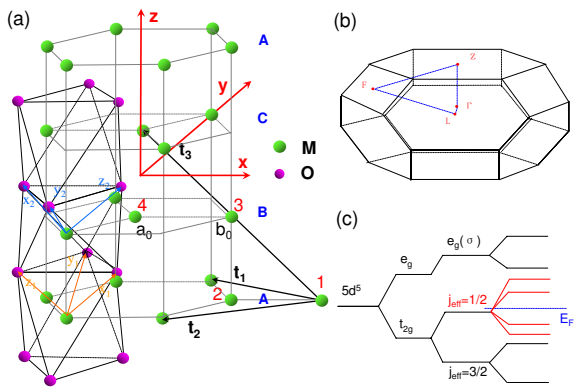

FIG. 1: (color online) (a) Corundum crystal structure with three primitive lattice vector denoted as $\vec{t}_{1,2,3}$. Each transition metal ion M (M=Ir, Os, etc.) (green large circles) is surrounded by oxygen octahedron (red small circles). Each unit cell has four M atoms, denoted as $1,2,3,4$. The space group is $R\bar{3}c$. (b) Brillouin zone for corundum structure with space group $R\bar{3}c$. The four inequivalent time-reversal invariant points are $\Gamma(000)$, $F(\pi 00)$, $L(\pi\pi\pi)$ and $Z(00\pi)$. (c) Schematic crystal field splitting of $5d$ level in corundum structure. We are interested in the half filling case with effective angular momentum $j_{\rm eff}=1/2$.

$j_{\rm eff}=1/2$ sub-bands. For example, the ions Fe^{3+}, Ir^{4+} etc with five d-electrons satisfy this requirement[23].

To obtain the electron dynamics in this system, we start by a symmetry analysis to the corundum structure. The space group of this structure is $D^5_{3d}(R\bar{3}c)$. It has a trigonal axis (three-fold rotation symmetry C_3) defined by z axis, a binary axis (two-fold rotation symmetry C_2), defined by y axis, and inversion symmetry with the inversion center at the middle of the two neighbor transition metal atoms. The primitive lattice vectors $\vec{t}_{1,2,3}$ and primitive unit cells are shown in Fig. 1(a), where each unit cell consists of four transition metal atoms denoted as 1,2,3,4. Since the oxygen p-level ϵ_p are far away from the Fermi level, we can consider a model describing only d-electrons, with the hopping mediated by the oxygen p-orbitals. The model is generally written as

$$\mathcal{H}_0=-\sum_{\langle ij\rangle}\left[d_i^\dagger t_{ij}d_j+h.c.\right]+\sum_{\langle\langle ij\rangle\rangle}\left[d_i^\dagger \hat{t}'_{ij}d_j+h.c.\right], \quad (2)$$

where $\langle ij\rangle$ and $\langle\langle ij\rangle\rangle$ denote the nearest-neighbor (NN) and next-nearest-neighbor (NNN) sites, respectively, and the hopping terms t_{ij} and $\hat{t}'_{ij}$ are in general 2×2 matrices. The form of the parameters $t_{ij},\hat{t}'_{ij}$ can be simplified by symmetry considerations. Due to space limitation, we will only present the result of the symmetry analysis. The NN transfer integral t_{ij} are real and spin independent, with two independent parameters, the intra-plane hopping t and the inter-plane hopping $t_\perp$. $t=(pd\pi)^2[(pp\sigma)+3(pp\pi)]/3(\epsilon_d-\epsilon_p)^2$ [17], where $(pd\pi)$, $(pp\sigma)$, and $(pp\pi)$ are Slater-Koster parameters between pd and pp, respectively [25]. The contribution of the order of $(pd\pi)^2/(\epsilon_d-\epsilon_p)$ cancel out in the honeycomb lattice, in sharp contrast to Sr_2IrO_4 with the perovskite lattice [26, 27]. The NNN transfer integrals are spin dependent, and it is essential for the realization of the topological insulator phase. For intra-plane in layer A, $1\rightarrow 1$ hopping can be written as

$$\hat{t}'_{11} \;=\; it'_{1\parallel}\vec{\sigma}\cdot\vec{r}_{11}+t_{1\parallel}, \quad (3)$$

$\vec{r}_{11}$ is a unit vector $\vec{r}_{11}\propto\vec{t}_{11}+1/\sqrt{2}\hat{z}$, $\vec{t}_{11}$ is the hopping link. $\hat{t}'_{22}=\hat{t}'^{\dagger}_{11}$ due to inversion symmetry. While in B plane, $\hat{t}'_{33}=e^{-i\pi/2\sigma_z}\hat{t}'_{11}e^{i\pi/2\sigma_z}$, $\hat{t}'_{44}=e^{-i\pi/2\sigma_z}\hat{t}'_{22}e^{i\pi/2\sigma_z}$ due to C_2 symmetry. For inter-plane ($A\rightarrow B$),

$$\hat{t}'_{13}=it'_{2\perp}\vec{\sigma}\cdot\vec{r}_{13}+t_{2\perp} \quad (4)$$

$\vec{r}_{13}$ is a unit vector $\vec{r}_{13}\propto\vec{t}_{13}-\alpha\hat{z}$, $\vec{t}_{13}$ is the hopping link, α is some parameter which depend on materials and cannot be determined purely by symmetry, below we choose $\alpha=1/\sqrt{2}$ which has almost the same amplitude as intra-plane. $\hat{t}'_{24}=\hat{t}'_{13}$, $\hat{t}'_{14}=\hat{t}'_{23}=e^{-i\pi/6\sigma_z}\hat{t}'_{13}e^{i\pi/6\sigma_z}$. Explicitly, $\vec{r}_{ij}$ for the intra-plane $1\rightarrow 1, 2\rightarrow 2$ hopping are x_1,y_1,z_1, and $3\rightarrow 3, 4\rightarrow 4$ are x_2,y_2,z_2 denoting in Fig. 1(a).

In summary, the transfer integrals are real and spin independent for NN links, while complex and spin dependent for NNN links. The accurate hopping parameters varies in different materials. As an example, in the following we will use the transfer integrals of Ir oxide introduced in Ref. [17]. One can always define all the parameters in the unit of in-plane NN hopping t, which leads to $t=1$, $t'_{1\parallel}=0.33$, $t_{1\parallel}=-0.1$, $t_\perp=y$, $t_{2\perp}=0.5y$, $t'_{2\perp}=\lambda t_{2\perp}=0.4y$. Here λ is the SOC strength which determines the ratio of spin-dependent hopping and spin-independent hopping. For Ir oxide we have $\lambda=0.8$. All the inter-plane hopping matrix elements are rescaled by a factor y which incorporates the anisotropy between intra-plane and inter-plane directions. The energy dispersion for $y=0.3$ (dashed line) and $y=0.55$ (solid line) are shown in Fig. 2(a), which shows that the system at half filling is an insulator in both case. Due to inversion symmetry, all the energy bands are doubly degenerate.

In three-dimensional topological band insulators, four independent Z_2 topological invariants can be defined [28–30]. For inversion symmetric systems, all the topological invariants can be simply determined by the parity of the wave-functions at the 8 time-reversal invariant momenta (TRIM) in the Brillouin zone [3]. $\mathbf{G}_1$, $\mathbf{G}_2$, $\mathbf{G}_3$ are the three basis vectors of the reciprocal lattice, then the 8 TRIM's are defined by $\mathbf{k}_i=(k_1\mathbf{G}_1+k_2\mathbf{G}_2+k_3\mathbf{G}_3)/2\pi$ with $k_1,k_2,k_3=0$ or π. For each TRIM $\mathbf{k}_i$, one can define a Z_2 quantity δ_i as the multiplication of the parity of all occupied bands $\delta_i=\prod_{s\in\rm occ}\xi_s$, with ξ_s the parity of s-th band. It should be noticed that a Kramers pair of bands are only counted once, otherwise δ_i would always be even. The four Z_2 invariants $(\nu_0;\nu_1\nu_2\nu_3)$ can

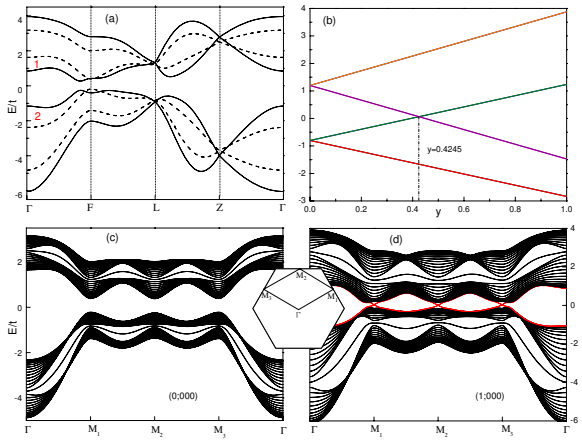

FIG. 2: (color online) (a) 3D energy band dispersion of tight-binding model for corundum structure with $\lambda = 0.8$, and $y = 0.3$(dashed line), $y = 0.55$(solid line). (b) The change of energy levels at F point ($\pi 00$) versus y. A band crossing occurs at $y = 0.4245$. The system changes from trivial insulator to topological insulator. (c) & (d) 2D band structure for a slab with 001 surface for the parameters $\lambda = 0.8$, $y = 0.3$ in (c) and $y = 0.55$ in (d). The red curves in (d) stands for surface states. The inset shows the surface Brillouin zone.

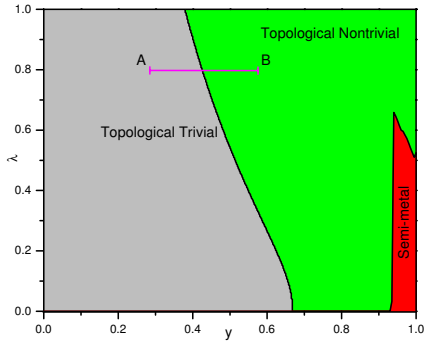

FIG. 3: (color online) The phase diagram of the system with two variables: the out of plane hopping parameter y and SOC parameter λ. The green and gray regions stand for topological nontrivial and trivial phases, respectively. Point A and B correspond to the parameters used in Fig. 2(c) and (d), respectively.

be determined by δ_i in which $\nu_0 = \prod_{i=1}^{8} \delta_i$ is the strong topological invariant which is stable upon disorder, and responsible for the topological magneto-electric effect[11]. More discussions on the other three "weak topological invariants" can be found in Ref.[3]. For $y = 0.3$, we find $\delta = +1$ at all TRIM at half filling. On the contrary, for $y = 0.55$ we find $\delta = -1$ at the three F points (see Fig. 1 (b)) and $\delta = +1$ at all other TRIM's. Consequently, $y = 0.55$ phase is a strong topological insulator(STI) with the topological character $(1; 000)$, and $y = 0.3$ is a trivial insulator with character $(0; 000)$. From this result we see that a band inversion[1] occurs at F points upon the change of y. In Fig. 2 (b) we show the energy at F point versus y, from which one can see clearly a level crossing at $y \simeq 0.42$. The topological invariants can be calculated for all values of anisotropy parameter y and SOC parameter λ, which leads to the phase diagram shown in Fig. 3. One can see that the topological nontrivial band structure can be realized at large y (i.e., small anisotropy) even for *infinitesimal* SOC. However, one should notice that for some parameters the band structure is actually a semi-metal (similar to Sb), which has a direct gap but does not have in-direct gap. We also solve the Hamiltonian (2) in a slab geometry with two 001 surfaces to study explicitly the topological surface states. Fig. 2(c)&(d) shows the 2D energy dispersion of the two systems shown in Fig. 2(a). In addition to the bulk states, for $y = 0.55$ there are surface states with three Dirac cones at M points of the surface BZ, while no surface state is found for $y = 0.3$, in consistency with the bulk topological invariants.

To get a better understanding of the physical properties of this system, a low energy effective model can be obtained by expanding the Hamiltonian around the F points. Around each F point, the effective model is 4×4 which describes two Kramers pairs of low lying bands and has Dirac-like form. In the following, we will denote the momentum by its coordinate in the basis of reciprocal lattice, *i.e.*, $\mathbf{k} = (k_1\mathbf{G}_1 + k_2\mathbf{G}_2 + k_3\mathbf{G}_3)/2\pi$. The F points are given by $(\pi, 0, 0)$, $(0, \pi, 0)$ and $(\pi, \pi, 0)$. Around the point $(\pi, 0, 0)$ the Hamiltonian has the following form:

$$\mathcal{H}_{\text{eff}}(\pi 00) = \epsilon_0(\mathbf{q})\mathbb{I}_{4\times 4} + \sum_{a=1}^{5} d_a(\mathbf{q})\Gamma_a, \qquad (5)$$

Here the Dirac Γ-matrices are defined as $\Gamma_a = (\tau_x \otimes \sigma_x, \tau_x \otimes \sigma_y, \tau_y \otimes 1, \tau_z \otimes 1, \tau_x \otimes \sigma_z)$ where τ_i and σ_i $(i = x, y, z)$ denote the Pauli matrices in the space of orbital and spin, respectively. $\mathbf{q} = \mathbf{k} - (\pi 00)$, $d_a(\mathbf{q}) = \sum_{i=1,2,3} A_i^a q_i$ for $a = 1, 2, 3, 5$, $d_4(\mathbf{q}) = M + \sum_{i=1,2,3} B_i q_i^2$, and $\epsilon_0(\mathbf{q}) = C + \sum_{i=1,2,3} D_i q_i^2$. For $\lambda = 0.8$, around the topological phase transition point we have

$$\begin{aligned} A_i^a &= \begin{pmatrix} 0.14 & -0.12 & 0.37 & -0.34 \\ -0.47 & 0.06 & -0.13 & 0.09 \\ 0.014 & 0.038 & 0.015 & 0.055 \end{pmatrix}, \\ B_i &= (0.625, 0.32, 0.24), \\ D_i &= (0.375, 0.04, 0.04) \end{aligned}$$

$C = 0.064$. The mass parameter M depends on y as $M \approx -23y + 9.76$ which changes sign at $y \simeq 0.42$ and leads to the topological phase transition. The effective Hamiltonian around the other two F points at $(0\pi 0)$ and $(\pi\pi 0)$ can be obtained by C_3 rotation.

Now we study the effect of electron correlation. The leading term in the interaction Hamiltonian is the on-site Hubbard repulsion for the $j_{\text{eff}} = 1/2$ orbitals $H_{\text{int}} = U \sum_i n_{i\uparrow} n_{i\downarrow}$. Magnetic ordering can be studied in mean

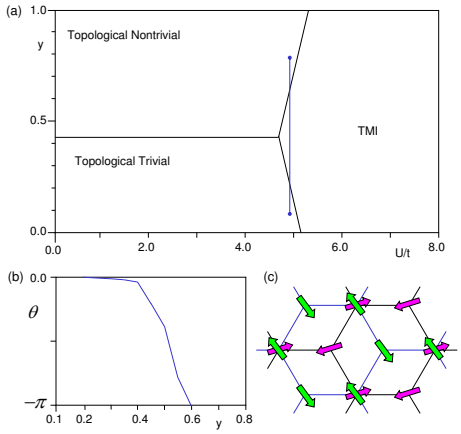

FIG. 4: (color online) (a) The phase diagram with y and U as parameters. (b) The value of θ along the blue line in the phase diagram. θ deviate from the TRI values 0 and π in the SDW phase for it breaks time-reversal symmetry $\mathcal{T}$ spontaneously. (c) The SDW order pattern. The purple arrows denote the spin in A layer and the green arrows denote the spin in the adjacent B layer. Other possible spin orderings can be obtained by six-fold rotations of this one.

field approximation. For simplicity, we only consider the order parameters that do not break translational symmetry. The mean-field calculation predicts a spin-density wave (SDW) phase above a critical U, and the spin moments of this SDW phase lie in the honeycomb plane, which are ordered antiferromagnetically within each layer and non-collinear between the two neighboring layers, as shown in Fig. 4. A finite mass for exciting the SDW phase is for example $m_{\rm SDW}/t = 3.65$ when $U/t = 6.0$. Experimentally, α-Fe_2O_3 develops a canted anti-ferromagnetic phase with spins residing in the honeycomb layer when $T_M < T < T_{\rm Néel}$, where T_M is the Morin transition temperature [31–33]. Spins in each layer are parallel, and those in two adjacent layers are coupled anti-ferromagnetically. Moreover, due to a slight spin-canting, the spins in adjacent layers are not exactly antiparallel (non-collinear). Spins can be ordered along one of three directions interchanged by C_3 and are homogeneously distributed in the crystal [31, 32]. The deviation from the SDW pattern may due to the hopping parameters chosen in the calculation [33]. Although it is different from the pattern we obtained in Fig. 4, the spin ordering in bulk α-Fe_2O_3 breaks $\mathcal{T}$, giving rise to $\theta \neq 0, \pi$. Therefore, α-Fe_2O_3 is a possible material to realize TMI.

The value of θ in the SDW phase of this effective model can be calculated as in Ref. [15]

$$\theta = \frac{1}{4\pi}\int d^3k \frac{2|d| + d_4}{(|d| + d_4)^2|d|^3}\epsilon^{ijkl} d_i \partial_x d_j \partial_y d_k \partial_z d_l, \quad (6)$$

where $i, j, k, l = 1, 2, 3, 5$, and $|d| = (\sum_{a=1}^{5} d_a^2)^{1/2}$. Since the main contribution to θ comes from the region close to Dirac points, θ can be approximated by the sum of θs calculated separately for each Dirac point using the effective model. The numerical results of θ is shown in Fig. 4 (b).

We wish to thank T. L. Hughes, Ian Fisher, Z. J. Xu and B. F. Zhu for insightful discussion. This work is supported by the NSF under grant numbers DMR-0904264 and by the Keck Foundation. JW acknowledges the support of China Scholarship Council, NSF of China (Grant No.10774086), and the Program of Basic Research Development of China (Grant No. 2006CB921500).

[1] B. A. Bernevig, T. L. Hughes, and S.C. Zhang, Science **314**, 1757 (2006).
[2] M. König *et al.*, Science **318**, 766 (2007).
[3] L. Fu and C. L. Kane, Phys. Rev. B **76**, 045302 (2007).
[4] D. Hsieh *et al.*, Nature **452**, 970 (2008).
[5] H. Zhang *et al.*, Nat. Phys. **5**, 438 (2009).
[6] Y. Xia *et al.*, Nat. Phys. **5**, 398 (2009).
[7] Y. L. Chen *et al.*, Science **325** (2009).
[8] X. L. Qi and S. C. Zhang, Phys. Today **63**, 33 (2010).
[9] M. Z. Hasan and C. L. Kane, Rev. Mod. Phys. **82**, 3045 (2010).
[10] F. Wilczek, Phys. Rev. Lett. **58**, 1799 (1987).
[11] X. L. Qi, T. L. Hughes, and S. C. Zhang, Phys. Rev. B **78**, 195424 (2008).
[12] W. K. Tse and A. H. MacDonald, Phys. Rev. Lett. **105**, 057401 (2010).
[13] J. Maciejko *et al.*, Phys. Rev. Lett. **105**, 166803 (2010).
[14] X. L. Qi, *et al.*, Science **323**, 1184 (2009).
[15] R. Li *et al.*, Nat. Phys. **6**, 284 (2010).
[16] S. Raghu *et al.*, Phys. Rev. Lett. **100**, 156401 (2008).
[17] A. Shitade *et al.*, Phys. Rev. Lett. **102**, 256403 (2009).
[18] H. M. Guo and M. Franz, Phys. Rev. Lett. **103**, 206805 (2009).
[19] D. Pesin and L. Balents, Nat. Phys. **6**, 376 (2010).
[20] Y. L. Chen *et al.*, Phys. Rev. Lett. **105**, 266401 (2010).
[21] S. Chadov *et al.*, Nat. Mat. **9**, 541 (2010).
[22] H. Lin *et al.*, Nat. Mat. **9**, 546 (2010).
[23] C. T. Prewitt *et al.*, Inorg. Chem. **8**, 1985 (1969).
[24] I. Nebenzahl and M. Weger, Phil. Mag. **24**, 1119 (1971).
[25] W. A. Harrison, *Elementary Electronic Structure* (World Scientific, Singapore, 1999).
[26] B. J. Kim *et al.*, Phys. Rev. Lett. **101**, 076402 (2008).
[27] B. J. Kim *et al.*, Science **323**, 1329 (2009).
[28] J. E. Moore and L. Balents, Phys. Rev. B **75**, 121306 (2007).
[29] L. Fu, C. L. Kane, and E. J. Mele, Phys. Rev. Lett. **98**, 106803 (2007).
[30] R. Roy, Phys. Rev. B **79**, 195322 (2009).
[31] M. Brunel and F. De Bergevin, Acta. Cryst. A**37**, 324 (1981).
[32] A. H. Morrish, *Canted Antiferromagnetism: Hermatite* (World Scientific, Singapore, 1994).
[33] M. Catti, G. Valerio, and R. Dovesi, Phys. Rev. B **51**, 7441 (1995).